

RSC Advances

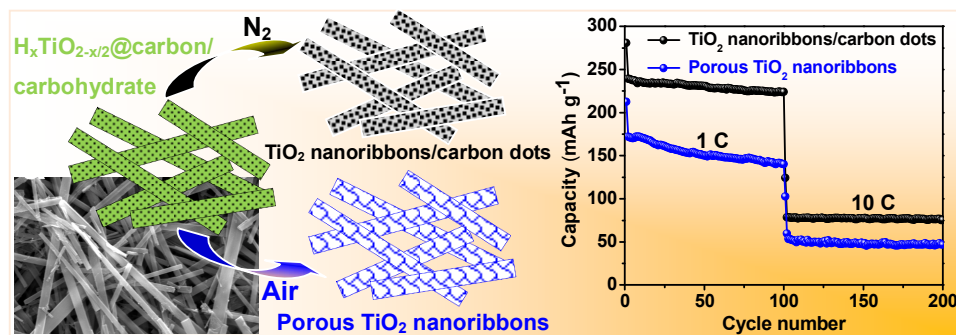


This is an *Accepted Manuscript*, which has been through the Royal Society of Chemistry peer review process and has been accepted for publication.

Accepted Manuscripts are published online shortly after acceptance, before technical editing, formatting and proof reading. Using this free service, authors can make their results available to the community, in citable form, before we publish the edited article. This *Accepted Manuscript* will be replaced by the edited, formatted and paginated article as soon as this is available.

You can find more information about *Accepted Manuscripts* in the [Information for Authors](#).

Please note that technical editing may introduce minor changes to the text and/or graphics, which may alter content. The journal's standard [Terms & Conditions](#) and the [Ethical guidelines](#) still apply. In no event shall the Royal Society of Chemistry be held responsible for any errors or omissions in this *Accepted Manuscript* or any consequences arising from the use of any information it contains.

Graphic

Porous TiO₂ nanoribbons and nano-composite of TiO₂ nanoribbons/carbon dots with excellent performance in lithium-ion battery were prepared *via* a simple and efficient method.

Cite this: DOI: 10.1039/c0xx00000x

www.rsc.org/xxxxxx

ARTICLE TYPE

Porous TiO₂ nanoribbons and TiO₂ nanoribbons/carbon dots composites for an enhanced Li-ion storage

Hai Ming,^{a, b, c, e} Yuerong Yan,^d Jun Ming,^{b, *} Xiaowei Li,^{a, c} Qun Zhou,^a Hui Huang,^{c, *} and Junwei Zheng^{a, *}

Received (in XXX, XXX) Xth XXXXXXXXX 20XX, Accepted Xth XXXXXXXXX 20XX

DOI: 10.1039/b000000x

Porous TiO₂ nanoribbons and TiO₂ nanoribbons/carbon dots composites with excellent performance in lithium-ion batteries were prepared via a simple and efficient method.

TiO₂ has attracted great attention as anode material in promising Li-ion battery (LIB) due to its low cost, excellent rate capability, and superior safety.¹⁻³ However, the wide application of TiO₂ was still limited by the low electron transport ability which always gave rise to a poor cycling performance at high discharge/charge rates.^{4,5} To solve this problem, preparing TiO₂ on nanoscale has been proven to be an efficient way to reduce the pathways of ions and electrons.^{6,7} However, the nanomaterials often self-aggregated seriously owing to the high surface energy, under which the effective contact areas with conductive additives and electrolyte was largely reduced in battery application. In this way, keeping the effective contact areas as large as we can and fully realizing the advantage of active materials at nanometer scale is still a challenge and of great importance. To date, considerable efforts have been made to explore a variety of TiO₂ with different nanostructures (e.g., sphere, porous, tube, wire, arrow, etc.)⁸⁻¹¹ and composite compositions (TiO₂/CNTs, TiO₂/Graphene, TiO₂/Fe₂O₃, TiO₂/Sn, etc.) to resolve the problem of poor rate capability and the strong trend of aggregation.¹²⁻¹⁵ Among these materials, the use of one dimensional (1D) TiO₂ nanostructures (rod, fiber, wire, tube, etc.) is a particularly efficient way to incorporate the advantageous characteristics of the material while achieving a desirable performance improvement.¹⁶ These 1D nanomaterials with a low degree of aggregation tendency could serve as anodes for LIBs from the following several aspects: (i) allowing a short Li-ion insertion/extraction distance; (ii) facilitating strain relaxation upon electrochemical cycling, (iii) providing a large ratio value of surface to volume to contact with the electrolyte, which can improve the capacity and cycle life of LIBs.¹⁷ Therefore, to some extent, such kind of hierarchical 1D nanomaterials are one of the most favorable structures as anode or cathode materials for high-performance LIBs.

Moreover, 1D TiO₂ nanomaterials with rich porosity or modified with carbon dots can ensure a better electrochemical performance. The porous structures are not only conducive to lower current densities at the electrode-electrolyte interface,¹⁸ but also beneficial to fully utilize high electrochemical reaction rates per unit volume¹⁹ and enhance diffusion kinetics by reducing the diffusion pathway for electronic and ionic transport.²⁰ Alternatively, the doping/modifying/implanting of carbon dots

into the matrix of TiO₂ could display a series of unique physical and chemical properties due to the intriguing characteristics of carbon dots,²¹ and also it could improve the electrochemical performance of TiO₂ significantly because they can narrow the band gap of TiO₂, reduce the polarization, enhance the conductivity, and increase the capacity stability.^{22,23} Furthermore, the introducing of carbon can also induce the formation of Ti³⁺ sites in the TiO₂ crystalline structure, improving the conductivity and structure stability, which can efficiently enhance the rate capability and cycling performance of the TiO₂ electrode.^{24,25} Most importantly, different from the traditional surface coating with carbon or loading into the matrix of carbon, embedding carbon-dots into the structure of TiO₂ could accelerate the transfer ability of electrons from the internal body to the surface of TiO₂.

Herein, we reported a simple method to prepare 1D porous TiO₂ nanoribbons (P-TNRs) and TiO₂ nanoribbons/carbon dots composites (TNRs/C) just varying the calcination condition. Compared to bulk TiO₂, they showed a largely improved performance as anode materials in LIB. For instance, P-TNRs, with porous structure (~8 nm) and high specific surface area (128 m² g⁻¹), exhibited a high capacity around 250 mAh g⁻¹ at the current rate of 0.1 C and reversible capacity over 138 mAh g⁻¹ after 100 cycles at 1 C (where define 1 C = 168 mAh g⁻¹, TiO₂ + xLi⁺ + xe⁻ → Li_xTiO₂, x = 0.5). While the TNRs/C that embedded with plentiful carbon dots (1-3 nm) successfully delivered a higher capacity around 300 mAh g⁻¹ at 0.1 C and a reversible

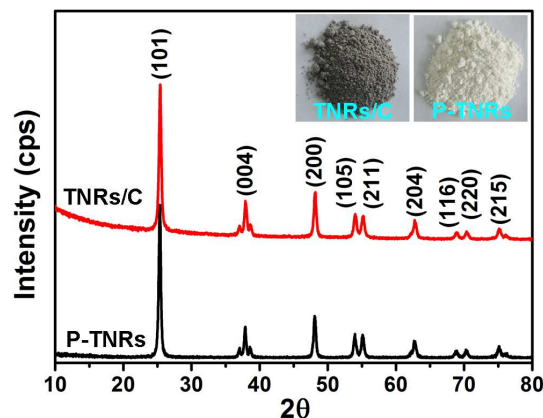


Fig. 1 (a) XRD patterns and digital images (insert) of P-TNRs and TNRs/C.

capacity over 225 mAh g⁻¹ after 100 cycles at 1 C. Furthermore, the resulting effects, caused by the embedding of carbon dots and introducing of porosity, on the electrochemical properties of the TiO₂ were comparatively investigated and discussed.

In a typical synthesis, 4 g glucose and 1 g TiO₂ was dissolved into a 10 M NaOH solution sufficiently, and then the solution was sealed in the Teflon-lined stainless steel autoclave and heated at 190 °C for 48 h. Finally, the as-prepared yellow-white intermediates was treated by HCl (pH = 1.0) and then calcined at 500 °C under a nitrogen atmosphere, giving rise to black TNRs/C. Based on the intermediates, P-TNRs could also be prepared readily under an air atmosphere. According to the X-ray powder diffraction (XRD) patterns, the crystalline structure of the TNRs/C and P-TNRs are both ascribed to the normal anatase TiO₂ (JCPDS Card No. 89-4921) (Fig. 1). However, they show quite different colors of black (TNRs/C) and white color (P-TNRs) respectively due to the embedding of carbon dots.

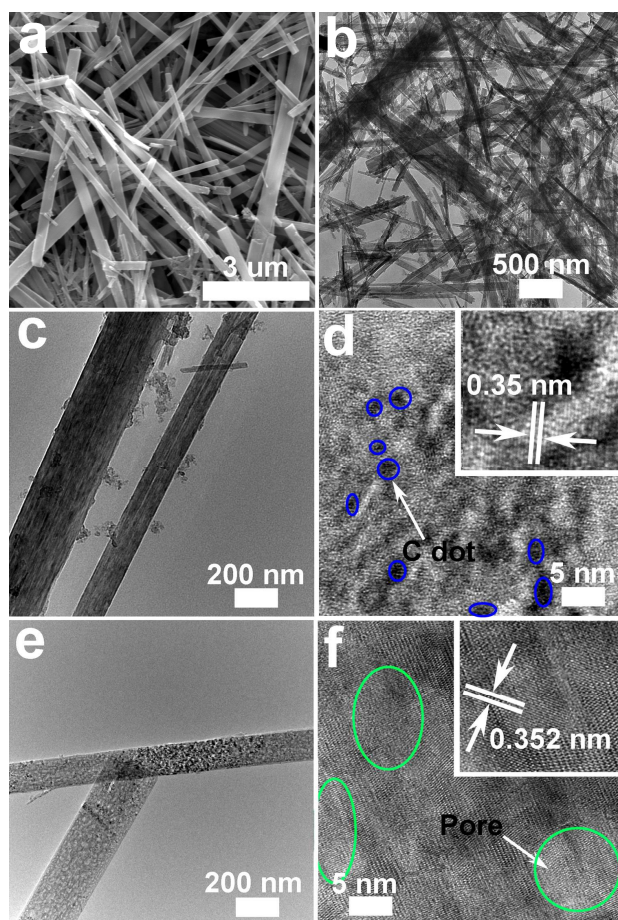


Fig. 2 (a) SEM and (b) TEM images of intermediates, (c) TEM and (d) HRTEM images of TNRs/C; (e) TEM and (f) HRTEM images of P-TNRs.

The intermediates have a uniform morphology of ribbon and a good distribution in diameter ranging from 100 to 300 nm, while its length could achieve several micro-meters, as shown in scanning electron microscopy (SEM) and transmission electron micrograph (TEM) (Fig. 2a, b). SEM images of TNRs/C and P-TNRs indicated that they can maintain the intermediates' morphology even after the calcination and also possess a

characteristic of nanoribbons with the length of several micrometers (Fig. S1). While the thickness of TNRs/C was about 52 nm, as confirmed by the atomic force microscope (AFM) image (Fig. S2), demonstrating that the nanoribbons have a high ratio of the length to width which is consistent with the character of 1D nanomaterials. The detail nanostructures of TNRs/C were also confirmed by the TEM and HRTEM (Fig. 2c and d). The diameter of the single TNRs/C nanoribbon is about 200 nm, and the amorphous C-dots with a diameter around 1-3 nm (marked by blue line) could be observed clearly in the structure of TiO₂. It is well-known that the carbon dots could be synthesized directly from glucose by a one-step alkali assisted ultrasonic treatment or hydrothermal treatment. Herein in this method, the carbon dots probably are resulted from two approaches of hydrothermal treatment and carbonization of residual glucose/intermediates of carbohydrates²⁶, as confirmed by the Fourier transform infrared (FTIR) (Fig. S3). Under the HRTEM (Fig. 2d), the lattice fringe with a spacing of 0.35 nm occupies most areas on TNRs/C, and it well corresponds to the spacing of (101) planes of TiO₂. The uniform distribution of elements of C, Ti, and O in the energy-dispersive X-ray spectrometry (EDS) mapping of single TNRs/C unambiguously confirmed that the carbon dots were indeed embedded in the structure of TiO₂ nanoribbons (Fig. S4). With varying the calcination conditions to air atmosphere for the intermediate, P-TNRs with porous structure could be obtained, as shown in the Fig. 2e. The diameter of the P-TNRs was about 200 nm and the length was also in micro-size distribution. The interplanar distance is 0.35 nm, which belongs to the facet of (101) planes of TiO₂. Notably, numerous pores with the diameter of 2 - 15 nm could be observed on the structure of the TNRs, directly confirming the porous characteristics of the P-TNRs.

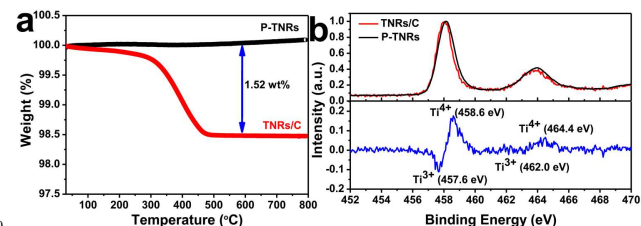


Fig. 3 (a) TGA data of the as-prepared TNRs/C and P-TNRs; (b) Overlay of normalized XPS high-resolution spectra of the Ti2p regions of the TNRs/C and P-TNRs, respectively.

The carbon content of as-prepared P-TNRs and TNRs/C were determined by the thermogravimetric analysis (TGA), as shown in Fig. 3a. The sample of TNRs/C shows a significant weight loss at 300 °C, which could be attributed to the combustion of carbon. Up to the temperature of 475 °C, the total weight loss of TNRs/C was 1.5 wt% while it is 0 wt% for the sample of P-TNRs. It is clear that there is no residual carbon in the sample of P-TNRs, while the carbon dots in TNRs/C could be easily burned under a low temperature of 300-475 °C. In addition, the high-resolution Ti2p X-ray Photoelectron Spectroscopy (XPS) of TNRs/C and P-TNRs were compared in Fig. 3b. Two broad peaks centered near 464.4 and 458.6 eV were well in accordance with the characteristic peaks of Ti 2p_{1/2} and Ti 2p_{3/2} of Ti⁴⁺ in both samples.²⁷ While a small negative shift can be observed in the peak of Ti2p for the sample of TNRs/C, and it well demonstrated a change in the structure which was caused by the embedding of

carbon dots. By subtracting the normalized Ti2p spectra of TNRs with P-TNRs, two extra peaks appeared at ~ 462.0 and ~ 457.6 eV, and they are attributed to Ti2p1/2 and Ti2p3/2 peaks of Ti^{3+} .²⁸ This confirmed that the Ti^{3+} sites were successful created in TNRs/C during the calcination under the reduction ability of glucose and C-dots (high degree calcination at $500^\circ C$ introduced the following reaction, $CO_xH_y + TiO_2 \rightarrow TiO_{2-n} + CO_m$). Moreover, the carbon dots formed in the structure of TiO_2 could react with TiO_2 to form a lot of chemical bonds such as Ti-O-C and Ti-C-O (Fig. S1), which could reduce the redox potential of TiO_2 and introduce a lot of active centers, and then they are good for the lithium ions storage.²⁹

Fig. 4a showed the N_2 adsorption-desorption isotherm of the TNRs/C sample. It might be categorized as a type III isotherm without a distinct hysteresis loop. This is conceivable because the conversion of residual glucose into carbon dots could cover and/or fill the porous structure of TNRs. As a result, a relatively low surface area of $57\text{ m}^2\text{ g}^{-1}$ was obtained. Oppositely, the N_2

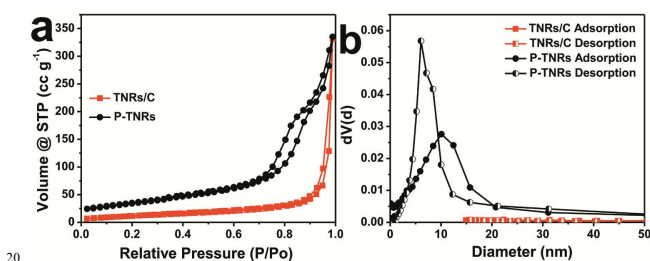


Fig. 4 (a) Nitrogen adsorption-desorption isotherm, (b) BJH pore size distribution plot of TNRs/C and P-TNRs.

adsorption-desorption isotherms curves (Fig. 4a) of P-TNRs showed a well-defined adsorption step and exhibited a typical type-IV isotherm, demonstrating the porous characteristic of the P-TNRs. The Brunauer-Emmett-Teller (BET) specific surface area and pore volume of the P-TNRs are $128\text{ m}^2\text{ g}^{-1}$ and $0.5\text{ cm}^3\text{ g}^{-1}$, respectively. In contrast to the sample of non-porous TNRs/C, the P-TNRs possess pores with a relative narrow diameter distribution ranging from 2-15 nm, as confirmed by the Barrett-Joyner-Halenda (BJH) pore size distribution. And the tap density of TNRs/C and P-TNRs are 0.66 and 0.60 g cm^{-3} , respectively, which were evaluated by the Autotap device (Quantachrom).

To circumstantiate the formative mechanism of TNRs/C and P-TNRs in the present reaction system, it could be interpreted as below based on the experimental route. At first, during the hydrothermal reaction process ($190^\circ C$, 24 h), the composite of $Na_2Ti_3O_7/C$ -carbohydrate with a morphology of ribbons could be obtained in the hydrothermal reaction of glucose and NaOH.¹⁶ And then, the as-prepared $Na_2Ti_3O_7/C$ nanoribbons were treated by HCl (pH = 1.0) to form the intermediates of $H_xTiO_{2-x/2}/C$ -carbohydrate. With calcination of these intermediates in the N_2 atmosphere, the $H_xTiO_{2-x/2}$ would be dehydrated and transform to TiO_2 , under which the carbon/residual carbohydrate could also be further carbonized to form high-conductive carbon dots. In this way, carbon dots were *in situ* encapsulated and/or embedded into the structure of TNRs. Alternatively calcination of the intermediates of $H_xTiO_{2-x/2}/C$ in the air atmosphere, the composite will dehydrate and transform to TiO_2 the same, but the

carbon-carbohydrate in H_xTiO_{2-x} could also be burned and then leave numerous pores in the structure of the TNRs.

The electrochemical performance of TNRs/C and P-TNRs in LIBs have been evaluated in half-cell test. The cyclic voltammograms (CV) of TNRs/C and P-TNRs from the 2nd cycle at a scan rate of 0.1 mV s^{-1} in the voltage range of 0.01 - 3.0 V were shown in Fig. 5a. The sharp oxidation peak at 1.70 V in the anodic scan and the reduction peak at about 2.0 V in the cathodic scan were associated with the Ti^{4+}/Ti^{3+} redox couple during lithium insertion and extraction.¹³ The anodic peak (2.04 V) of TNRs/C is more negative than that of P-TNRs (2.09 V), indicating a lower polarization coefficient the TNRs/C possess.¹⁸ Moreover, the current density and the integrated area of the TNRs/C are larger than that of P-TNRs, demonstrating that the carbon dots lead to a sufficient oxidation reaction process during the anodic cycling. Fig. 5b shows the 2nd rate charge/discharge curves for the TNRs/C and P-TNRs electrodes between 1.0 and 3.0 V at 0.05 C. Both curves are in good agreement with the CV analysis. Each discharge (lithium insertion) can be divided into three stages: (i) a fast decrease in voltage starting from the open-circuit potential to $\sim 1.7\text{ V}$; (ii) a quite long plateau region at $\sim 1.7\text{ V}$, reflecting the process of lithium insertion into the channels of crystal structure;

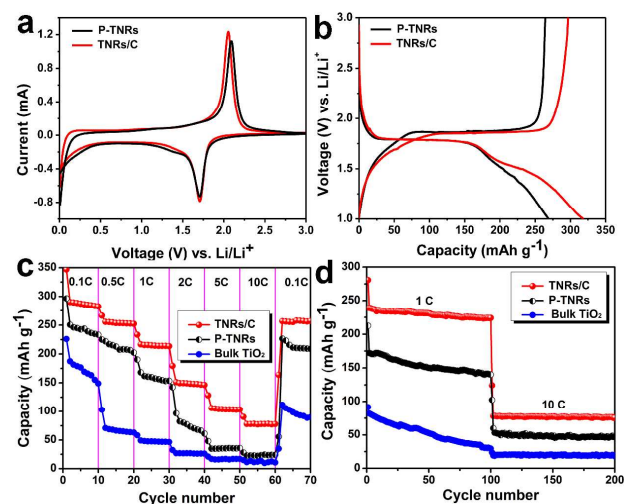


Fig. 5 (a) CV of TNRs/C and P-TNRs electrodes; (b) Voltage profiles of TNRs/C and P-TNR electrodes at the rate of 0.05 C; (c) different rates (0.1 - 10 C) (d) Cycling performances at 1 and 10 C of TNRs/C, P-TNR, and bulk TiO_2 electrodes.

(iii) a long gradual decay of the voltage after the plateau region, indicating the insertion of lithium ions into the microstructure of the material; Although P-TNRs have a larger surface area than that of TNRs/C, a much longer plateau of TNRs/C can be observed, indicating a rich interface (carbon dots/ TiO_2) existed in TNRs/C for lithium-ion storage. Due to the high degree of the redox reaction and the possible interfacial lithium storage (pseudo-capacitive effects),³⁰ a high capacity of 318 mAh g^{-1} can be delivered in the first discharge and then followed by a charge capacity of 297 mAh g^{-1} for the sample of TNRs/C, but they are only 269 and 264 mAh g^{-1} for P-TNRs. The TNRs/C electrode also exhibited a smaller separation between charge and discharge voltage plateaus, demonstrating the advanced structure possesses lower electrochemical polarization and

induces a better reversibility during the discharge/charge processes.³¹ A comparative results of rate capability was shown in Fig. 5c. In contrast to the P-TNRs and bulk TiO₂, the TNRs/C demonstrated a better performance. It delivered discharge capacities over 283, 250, 212, 146, 104 and 77 mAh g⁻¹ at the rates of 0.1 C, 0.5 C, 1 C, 2 C, 5 C and 10 C respectively, and finally recovered to around 256 mAh g⁻¹ at 0.1 C. Fig. 5d shows the cyclability of the TNRs/C, P-TNRs, and bulk TiO₂ electrodes at 1 and 10 C, respectively. The TNRs/C electrode showed an excellent cyclic performance and a high reversible specific capacity of over 225 and 73 mAh g⁻¹ after the 100 and 200 cycles, and it is much higher than the electrode of the P-TNRs (~138 and 45 mAh g⁻¹) and bulk TiO₂ (~30 and 19 mAh g⁻¹). The SEM images of TNRs/C and P-TNRs electrode after 20 cycles at the rate of 0.1 C showed that their morphology was similar to that before cycling and without any obvious aggregation, demonstrating a high structural stability of TNRs during the charge/discharge owing to the small volume variation of TiO₂ less than 4%.¹⁻³ Simply compare to other TiO₂-based materials reported before, the materials of TNRs/C demonstrated a higher capacity at the rate of 1C (Table S1).

To interpret the results, herein we built several models of electronic transfer route in the composite of C-TiO₂ to interpret the high performance of materials, except the advantages of 1D structures. The electrode consisting of active materials, binder of PVDF, and conductive material of Super P with a mass ratio of 8:1:1 was casted on copper foil, as illustrated in Fig. 6a. Generally for the normal bulk TiO₂, it is a well-known semiconductor with a low electronic conductivity (~10⁻⁹ S cm⁻¹), and therefore the rate of internal electrons transferring from TiO₂ to the Super P&PVDF should be very slow (Fig. 6b). Alternatively, numerous traditional works focused on coating the TiO₂ with a layer of carbon. In this way, it can improve the electrochemical performance of TiO₂@C because the electrons could transfer to the walls of carbon in any directions (Fig. 6c). But the enhancement was limited because the transfer rate of electrons from internal TiO₂ to the walls of carbon was still low if the particle of TiO₂ was little big. To short the transfer route of electrons in the structure of TiO₂, in this work we introduced the composite of carbon dots embedded into the TiO₂, that is, TNRs/C. As shown in Fig. 6d, the electrons could transfer easily in a short distance *via* a net-work, which undoubtedly could make the internal electrons transfer conveniently to the Super P&PVDF soon.³² The increased electronic conductivity of 3.19×10⁻³ S cm⁻¹ was well accordance with the speculation. Although the transfer rate of electrons were enhanced, it would be better to further coat the TiO₂/carbon dots with a layer of carbon (Fig. 6e), because in this way the electrons could transfer to any directions to the walls of carbon layer, which is another promising candidate for anode. The disadvantage of porous TiO₂ nanoribbons could be easily observed from the transfer route of electrons (Fig. 6f). Numerous porosity inevitably could be a barrier for the transfer of electrons, but the porous characteristic of materials could also enhance the contact areas with Super P&PVDF (Fig. 6f), as well as the electrolyte. So, it is a

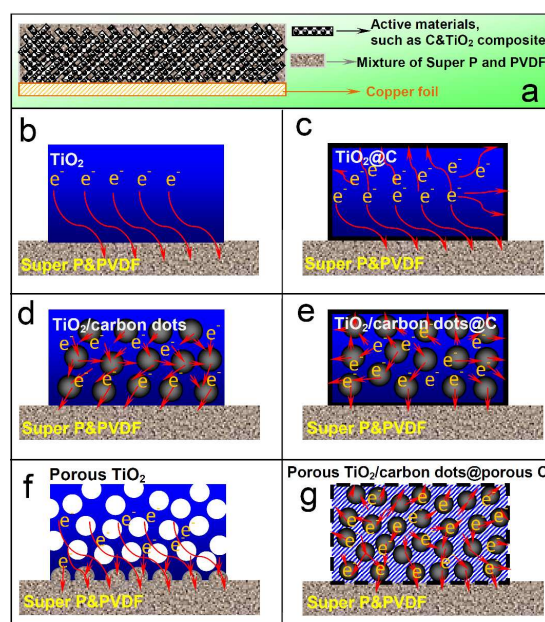


Fig. 6 (a) Model of casted electrode on copper foil. Probable electronic transfer route in the materials of (b) TiO₂, (c) TiO₂@C, (d) TiO₂/carbon dots, (e) TiO₂/carbon dots@C, (f) porous TiO₂ and porous TiO₂/carbon dots@porous C.

conflict and a balance between the porosity and conductivity should be controlled. However, the electrode conductivity of P-TNRs still showed a higher electronic conductivity (2.75×10⁻⁵ S cm⁻¹) than that of bulk TiO₂ (1.24×10⁻⁶ S cm⁻¹), which should be ascribed to the smaller size and specific structure of nanoribbons. This could well interpret that P-TNRs showed a high capacity than bulk TiO₂ but a lower capacity than that of TNRs/C. The higher conductivity of TNRs/C than that of P-TNRs was also proved by the electrochemical impedance spectroscopy (EIS) Nyquist plots (Fig. S6). Based on the analysis of results, an ideal structure of ordered porous TiO₂/carbon dots@porous C with a one dimensional structure was presented (Fig. 6g), which should be good for the transfer ability of electrons *via* a net-work consisting of carbon dots and also adsorbing enough electrolyte for the up/take of lithium ions. Relative researches about such advanced materials deserve to be further investigated.

In summary, a one-step strategy to prepare porous TiO₂ nanoribbons and TiO₂ nanoribbons/carbon dots composites with a narrow size distribution and uniform morphology was successfully developed. The probable mechanism of forming porosity and composite structure were discussed. As an anode material for LIBs, P-TNRs with the porous structures (~8 nm) and high specific surface area (128 m² g⁻¹) are capable of a high capacity around 250 mAh g⁻¹ at the current rate of 0.1 C and reversible capacity over 138 mAh g⁻¹ after 100 cycles at 1 C. In addition, TNRs/C that embedded with abundant carbon dots (1-3 nm) could deliver a higher capacity around 300 mAh g⁻¹ at the rate of 0.1 C and a reversible capacity over 225 mAh g⁻¹ after 100 cycles at 1 C. This dramatic improvement was attributed to the optimization of materials design in structure and/or compositions,

which can advance similar investigations for other kind of metal oxide (e.g., FeO_x, CoO_x, NiO_x, MnO_x) as anode materials. Moreover, this kind of 1D dimensional porous TiO₂ nanoribbons and TiO₂ nanoribbons/carbon dots composites could also be widely applied in other areas of catalysis, electrochemistry, photo-electronics and materials science. The analysis of introduced models of electronic transfer routes in the metal oxide-carbon composite could be expanded and also be significant for designing new advanced materials.

Financial supports from the Nature Science Foundation of China (Nos. 20873089, 20975073), Nature Science Foundation of Jiangsu Province (Nos. BK2011272), Industry-Academia Cooperation Innovation Fund Projects of Jiangsu Province (Nos. BY2011130), Key Laboratory of Lithium Ion Battery Materials of Jiangsu Province, China Scholarship Council (File. No. 201306920005) and Graduate Research and Innovation Projects in Jiangsu Province (CXZZ13_0802) are gratefully acknowledged.

Notes and references

^a College of Chemistry, Chemical Engineering and Materials Science, Soochow University, Suzhou 215123, P. R. China. E-mail: jwzheng@suda.edu.cn;

^b Department of Energy Engineering, Hanyang University, Seoul, 133-791, Republic of Korea; E-mail: mingjun6297@gmail.com

^c Institute of Functional Nano & Soft Materials (FUNSOM) and Jiangsu Key, Laboratory for Carbon Based Functional Materials & Devices, Soochow University, Suzhou, Jiangsu 215123, P. R. China. E-mail: hhuang0618@suda.edu.cn

^d Department of Science and Technology, Jiaozuo Teachers College, Jiaozuo, 454000, P. R. China.

^e Institute of Chemical Power Sources, Soochow University, Suzhou 215006 (P. R. China).

† Electronic Supplementary Information (ESI) available: Materials and Characterization. SEM images of TNRs/C, P-TNRs and their electrode before and after cycling. AFM image of TNRs/C. FTIR of TNRs/C, P-TNRs and their intermediates. Comparative performance of P-TNRs, TNRs/C and other TiO₂-based materials in previous literatures. Nyquist plots of TNRs/C and P-TNRs electrodes. See DOI: 10.1039/b000000x/

- 1 J. S. Chen, Y. L. Tan, C. M. Li, Y. L. Cheah, D. Luan, S. Madhavi, F. Y. C. Boey, L. A. Archer and X. W. Lou, *J. Am. Chem. Soc.*, 2010, **132**, 6124.
- 2 K. Saravanan, K. Ananthanarayanan and P. Balaya, *Energ. Environ. Sci.*, 2010, **3**, 939.
- 3 S. T. Myung, N. Takahashi, S. Komaba, C. S. Yoon, Y. K. Sun, K. Amine and H. Yashiro, *Adv. Funct. Mater.*, 2011, **21**, 3231.
- 4 G. N. Zhu, Y. G. Wang and Y. Y. Xia, *Energy Environ. Sci.*, 2012, **5**, 6652.
- 5 Y. S. Hu, Y. G. Guo, W. Sigle, S. Hore, P. Balaya and J. Maier, *Nat. Mater.*, 2006, **5**, 713.
- 6 C. Natarajan, K. Setoguchi and G. Nogami, *Electrochim. Acta*, 1998, **43**, 3371; Y. Ren, Z. Liu, F. Pourpoint, A. R. Armstrong, A. Robert Armstrong, C. P. Grey and P. G. Bruce, *Angew. Chem., Int. Ed.*, 2012, **51**, 2164.
- 7 J. Wang, Y. K. Zhou, Y. Y. Hu, R. Hayre and Z. P. Shao, *J. Phys. Chem. C*, 2011, **115**, 2529.
- 8 Y. Wang, X. W. Su and S. Lu, *J. Mater. Chem.*, 2012, **22**, 1969.
- 9 S. H. Liu, H. P. Jia, L. Han, J. L. Wang, P. F. Gao, D. D. Xu, J. Yang, and S. A. Che, *Adv. Mater.*, 2012, **24**, 3201.
- 10 H. S. Liu, Z. H. Bi, X. G. Sun, R. R. Unocic, M. P. Paranthaman, S. Dai and G. M. Brown, *Adv. Mater.*, 2011, **23**, 3450.
- 11 S-W. Kim, T. H. Han, J. Kim, H. Gwon, H-S. Moon, S-W. Kang, S. O. Kim and K. Kang, *ACS Nano*, 2009, **3**, 1085.

- 12 S. J. Ding, J. S. Chen, D. Y. Luan, F. Y. C. Boey, S. Madhavi and X. W. Lou, *Chem. Commun.*, 2011, **47**, 5780; Q. Wang, Z. H. Wen and J. H. Li, *Adv. Funct. Mater.*, 2006, **16**, 2141.
- 13 Z. X. Yang, G. D. Du, Q. Meng, Z. P. Guo, X. B. Yu, Z. X. Chen, T. L. Guo and R. Zeng, *J. Mater. Chem.*, 2012, **22**, 5848; J. Ming, Y. Wu, S. Nagarajan, D. J. Lee, Y. K. Sun and F. Y. Zhao, *J. Mater. Chem.* 2012, **22**, 22135.
- 14 Y. S. Luo, J. S. Luo, J. Jiang, W. W. Zhou, H. P. Yang, X. Y. Qi, H. Zhang, H. J. Fan, D. Y. W. Yu, C. M. Li and T. Yu, *Energy Environ. Sci.*, 2012, **5**, 6559.
- 15 Z. Y. Peng, Z. Shi and M. L. Liu, *Chem. Commun.*, 2000, 2125; H-G. Jung, C. S. Yoon, J. Prakash and Y. K. Sun, *J. Phys. Chem. C*, 2009, **113**, 21258; L. Zhao, Y. S. Hu, H. Li, Z. X. Wang and L. Q. Chen, *Adv. Mater.*, 2011, **23**, 1385; Y. G. Guo, Y. S. Hu and J. Maier, *Chem. Commun.*, 2006, 2783; L. F. Shen, C. Z. Yuan, H. J. Luo, X. G. Zhang, K. Xu and Y. Y. Xia, *J. Mater. Chem.*, 2010, **20**, 6998.
- 16 S. Bruttì, V. Gentili, H. Menard, B. Scrosati and P. G. Bruce, *Adv. Energy Mater.*, 2012, **2**, 322; J. W. Xu, C. H. Jia, B. Cao and W. F. Zhang, *Electrochim. Acta*, 2007, **52**, 8044; Z. X. Yang, G. D. Du, Z. P. Guo, X. B. Yu, Z. X. Chen, T. L. Guo, N. Sharma and H. K. Liu, *Electrochem. Commun.*, 2011, **13**, 46.
- 17 T. Brezesinski, J. Wang, S. H. Tolbert and B. Dunn, *Nat. Mater.*, 2010, **9**, 146. B. Tian, P. Xie, T. J. Kempa, D. C. Bell and C. M. Lieber, *Nat. Nanotechnol.*, 2009, **4**, 824. J. Ge, Y. Hu, M. Biasini, W. P. Beyermann and Y. Yin, *Angew. Chem., Int. Ed.*, 2007, **46**, 4342; J. Ge, Q. Zhang, T. Zhang and Y. Yin, *Angew. Chem., Int. Ed.*, 2008, **47**, 8924.
- 18 H. Ming, X. W. Li, Q. Zhou, M. M. Liu, L. L. Su, L. J. Bu, Z. H. Kang and J. W. Zheng, *New J. Chem.*, 2013, **37**, 1912.
- 19 A. Neubrand, *J. Appl. Electrochem.*, 1998, **28**, 1179.
- 20 Y. G. Guo, Y. S. Hu and J. Maier, *Chem. Commun.*, 2006, 2783.
- 21 H. Ming, Z. Ma, Y. Liu, K. M. Pan, H. Yu, F. Wang and Z. H. Kang, *Dalton Trans.*, 2012, **41**, 9526.
- 22 Y. M. Lin, R. K. Nagarale, K. C. Klavetter, A. Heller and C. B. Mullins, *J. Mater. Chem.*, 2012, **22**, 11134; Z. X. Yang, G. D. Du, Q. Meng, Z. P. Guo, X. B. Yu, Z. X. Chen, T. L. Guo and R. Zeng, *J. Mater. Chem.*, 2012, **22**, 5848; J. W. Zhang, X. X. Yan, J. W. Zhang, W. Cai, Z. S. Wu and Z. J. Zhang, *J. Power Sources*, 2012, **198**, 223.
- 23 H. Han, T. Song, J. Y. Bae, L. F. Nazar, H. Kim and U. Paik, *Energy Environ. Sci.*, 2011, **4**, 4532. H. Ming, X. W. Li, L. L. Su, M. M. Liu, L. L. Jin, L. J. Bu, Z. H. Kang and J. W. Zheng, *RSC Adv.*, 2013, **3**, 3836.
- 24 L. F. Shen, E. Uchaker, X. G. Zhang and G. Z. Cao, *Adv. Mater.*, 2012, **24**, 6502; F. X. Wu, Z. X. Wang, X. H. Li and H. J. Guo, *J. Mater. Chem.*, 2011, **21**, 12675.
- 25 X. H. Lu, G. M. Wang, T. Zhai, M. H. Yu, J. Y. Gan, Y. X. Tong and Y. Li, *Nano Lett.*, 2012, **12**, 1690; X. H. Lu, G. M. Wang, T. Zhai, M. H. Yu, S. L. Xie, Y. C. Ling, C. L. Liang, Y. X. Tong and Y. Li, *Nano Lett.*, 2012, **12**, 5376.
- 26 X. M. Sun and Y. D. Li, *Angew. Chem. Int. Ed.*, 2004, **43**, 597; H. T. Lia, X. D. He, Y. Liu, H. Huang, S. Y. Lian, S-T Lee and Z. H. Kang, *Carbon*, 2011, **49**, 605; J. Ming, R. Liu, G. Liang, H. Cheng, Y. Yu and F. Zhao, *J. Mater. Chem.* 2011, **21**, 10929.
- 27 X. Chen, L. Liu, P. Y. Yu and S. S. Mao, *Science*, 2011, **331**, 746; G. M. Wang, H. Wang, Y. Ling, Y. Tang, X. Yang, R. C. Fitzmorris, C. Wang, J. Z. Zhang and Y. Li, *Nano Lett.*, 2011, **11**, 3026.
- 28 Y. Liu, J. M. Szeifert, J. M. Feckl, B. Mandlmeier, J. Rathousky, O. Hayden, D. Fattakhova-Rohlfing and T. Bein, *ACS Nano*, 2010, **4**, 5373.
- 29 J-Y. Shin, J. H. Joo, D. Samuelis and J. Maier, *Chem. Mater.*, 2012, **24**, 543.
- 30 J. Wang, J. Polleux, J. Lim and B. Dunn, *J. Phys. Chem. C*, 2007, **111**, 14925.
- 31 D. Deng, M. G. Kim, J. Y. Lee and J. Cho, *Energy Environ. Sci.*, 2009, **2**, 818.
- 32 J. W. Xu, Y. F. Wang, Z. H. Li and W. F. Zhang, *J. Power Sources*, 2008, **175**, 903; V. G. Pol, S-H Kang, J. M. Calderon-Moreno, C. S. Johnson and M. M. Thackeray, *J. Power Sources*, 2010, **195**, 5039; J. S. Chen, Z. Y. Wang, X. C. Dong, P. Chen and X. W. Lou, *Nanoscale*, 2011, **3**, 2158.